Desalination and Water Treatment
www.deswater.com

doi: 10.5004/dwt.2019.23931

155 (2019) 32–47
July

Evolutionary prediction of an inclined dense jet in shallow water

Hossein Bonakdari*, Abdolmajid Mohammadian

Department of Civil Engineering, University of Ottawa, 161 Louis Pasteur, CBY A114,Ottawa, ON K1N 6N5, Canada, Tel. +1 (613)-562–5800 ext. 6492; Fax: +1 (613)-562–5173; emails: bonakdari@yahoo.com (H. Bonakdari), amohamma@uottawa.ca (A. Mohammadian)

Received 21 July 2017; Accepted 9 February 2019

ABSTRACT

Although several experiments have been done on inclined dense jets in shallow water where inclined dense jet interacts with the water surface, the jet trajectory and minimum dilution at the return point (S_r) and water surface (S_s) have not been generally formulated and reported. In this paper, new evolutionary-based models are developed to predict variables describing jet trajectory and dilution, including the non-dimensional horizontal displacement of the return point (x_r/D), non-dimensional horizontal displacement of the minimum surface dilution point (x_s/D), dilution at the return point (S_r) and minimum dilution at the water surface (S_s). These parameters are essential in brine discharge system design. Two sets of experimental data are applied to develop and evaluate the models, and the model networks are optimized using gene expression programming (GEP). The mentioned parameters serve to compute dilution and displacement at the return point and water surface as a function of discharge angle (θ), non-dimensional ambient depth (H/D) and jet densimetric Froude number (F). Partial derivative sensitivity analysis is also carried out to examine the effect of each dimensionless input variable on the target parameters. The explicit equations and pseudo codes reported facilitate easy estimation of the trajectory maximum impact point distance as well as dilutions for dense jets at different angles from the horizontal.

Keywords: Dilution; Inclined dense jet; Sensitivity analysis; Coastal water

1. Introduction

In recent years, desalinated seawater has become an alternative non-conventional source of freshwater. In many countries, this is considered a reliable and economically sustainable water resource. This treatment process produces brine with highly concentrated salt as waste that may be toxic to the water in which it is discharged and should therefore be diluted before discharge [1]. As the brine produced by desalination plants is disposed by discharge, it comes in direct contact with aquatic species via submerged inclined outfalls. This configuration is usually adopted for brine discharge in coastal waters through inclined dense jets with long curvilinear trajectories. Dense brine effluent with high salt concentration increases turbidity and has considerable environmental impact on surrounding coastal waters [2]. This effect is mainly seen in the vicinity of concentrated brine discharge pipes [3]. Because the effluent should mix well and efficiently in seawater [4], inclined jets acting as high-velocity turbulent jets should discharge the effluent upward [5]. Dilution reduces concentration, so the effluent can reach levels safe for entering marine or estuarine environments. An inclined dense jet follows a curvilinear trajectory by rising up to a maximum height and falling back toward the seabed (see Fig. 1). Following contact with the bottom, the diluted effluent spreads as a density current. In outfall design, it is commonly desirable for the outfall to be located close to the shore for maintenance reasons and cost minimization. In the case of shallow water areas, it is conceivable that the inclined dense jet impacts the water surface. Abessi and Roberts [13] considered the non-dimensional

* Corresponding author.

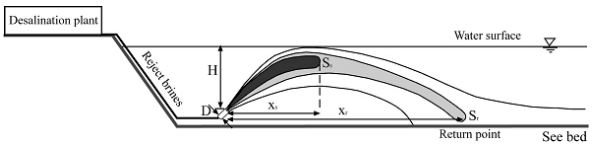

Fig. 1. Schematic side view of brine discharge from a desalination plant outfall.

parameter dF/H (where d is the nozzle diameter, F is the jet densimetric Froude number and H is the water depth) to identify the flow regime. The authors proposed that the values of dF/H less than 0.84, 0.48 and 0.42 lead to the fully submerged or the deep flow regime otherwise the jet is in surface contact and shallow flow regimes for θ = 30, 45 and 60 respectively. In terms of the physical features associated with a dense jet in shallow water, it is necessary to have detailed knowledge of the jet trajectory and dilution for outfall design and environmental impact assessment.

Many experimental and analytical studies have been carried out to investigate the behavior of inclined dense jets. Zeitoun et al. [6], Pincince and List [1], Roberts and Toms [7], Roberts et al. [5], Jirka [8], Cipollina et al. [9], Kikkert et al. [10], Shao and Law [11], Lai and Lee [12], Jiang et al. [4] and Abessi and Roberts [13] carried out experimental studies to describe the geometric features and dilution characteristics of inclined jets and developed a number of guidelines. According to Zeitoun et al.'s [6] experimental results, a 60° inclination relative to the horizontal axis produces maximum dilution before the jet impacts the sea bed. As the jet peak height is relatively large for a 60° inclination, in shallow coastal water regions smaller inclinations are more feasible. Accordingly, several studies have extended experimental investigations of 30° and 45° inclined dense jets. Therefore, depending on costal conditions, all three inclinations mentioned are applicable in practical cases. Bashitialshaaer et al. [14] performed an experimental investigation of negatively inclined buoyant jets to measure the geometric features describing the jet trajectory by performing 72 tests at 3 inclination angles (30°, 45° and 60°). Jiang et al. [4] carried out extensive experiments on inclined dense jets in a shallow ambient water environment to study the curvilinear jet trajectory and dilution at the water surface and near the sea bed with 30° and 45° inclined dense jets in shallow water. The nozzle diameter was 5.8 mm and the nozzle tip was located 5 cm above the bottom. The densimetric Froude number (F) of the jet was between 5 and 34.8 in all 42 tests. The most effective parameters considered in each experiment were the densimetric Froude number and non-dimensional water depth. The planar laser-induced fluorescence and particle image velocimetry methods were applied to measure the velocity and concentration distribution of the inclined dense jets. The study also presented an evaluation of the free surface impact on dilution. Abessi and Roberts [13] conducted vast experiments on 30°, 45° and 60° inclined dense jets in both deep and shallow water. The spatial variations of the jet trajectory and concentration were measured by three-dimensional laser-induced fluorescence. The water tank density was 998.2 kg/m^3 and the effluent density was either 1,014 or 1,021 kg/m^3. The jet's densimetric Froude number (F) varied between 18.8 and 82.5. The nozzle diameter was 0.317 cm and the nozzle was placed about 1.4–2 cm from the bottom.

Besides experimental studies, analytical solutions have also been investigated. For example, Cipollina et al. [15–16], Nikiforakis et al. [17] and Kikkert et al. [18] developed analytical solutions based on mass and momentum balance equations to predict the behavior of inclined dense jets. More recently, computational fluid dynamics (CFD) modeling of the behavior of inclined dense jets has gained tremendous attention. Some researchers have applied commercial CFD codes [19–24] and others have developed finite volume models to solve the governing equations numerically [25–26]. Such three-dimensional modeling tools facilitate good prediction of dense jet curvilinear trajectories but are too complicated for practical applications. In addition, result validation and verification require experimental results that restrict application in practical cases [27].

In recent years, artificial intelligence (AI) has been utilized in different fields as a powerful tool for modeling and solving complex nonlinear problems. In a number of hydraulic studies, gene expression programming (GEP) has been applied to predict various parameters. Azamathulla [28] predicted the scour depth downstream of sills using GEP. The study indicated that the proposed GEP approach produces more adequate results compared with existing equations. Ebtehaj et al. [29] employed GEP to estimate the side weir discharge coefficient. The authors performed a sensitivity analysis of the GEP models and concluded that the ratio of weir length to the depth of the upstream flow is the most effective parameter on the prediction results. The proposed equation also outperformed existing literature equations. Gholami et al. [30] developed a model based on GEP and used polar coordinates and discharge to propose a practical equation for the velocity field in a 90° channel bend. Moreover, Azimi et al. [31] extensively studied the discharge coefficient of side weirs using GEP. The authors proposed an explicit equation for use in practical, real-world engineering applications. Khozani et al. [32] were the first to propose an equation based on GEP for evaluating the shear stress distribution along the wetted perimeter of a circular open channel.

To the best of the authors' knowledge, GEP has never been used to determine variables that describe the trajectory and dilution of an inclined dense jet. In addition, despite advances in both experimental and numerical modeling of inclined jets, some challenges remain regarding design improvement considerations [33]. The return point distance from the nozzle jet and dilution at this point are vital design parameters to protect the sea floor against erosion caused by effluent. The horizontal displacement of the minimum surface dilution point and dilution at this point are thus crucial for environmental protection purposes. In particular, a general formulation of a jet trajectory and the minimum dilution at the return point and water surface is required, which is directly applicable to outfall systems. Consequently, a model that correlates the crucial dilution parameters and geometric jet features with the flow parameters is necessary. For this reason, the aim of the present study is to introduce a model that is capable of correlating the input and output values.

By using GEP four different equations are derived for evaluating the jet trajectory and dilution variables, i.e. the non-dimensional horizontal displacement of the return point (x_r/D), non-dimensional horizontal displacement of the minimum surface dilution point (x_s/D), dilution at the return

point (S_r) and minimum water surface dilution at the centerline maximum height (S_s) in terms of the three main parameters governing dense jet discharge in shallow water, namely the jet's densimetric Froude number (F), the non-dimensional depth (H/D) the discharge angle (θ). To this end, two comprehensive datasets for inclined dense jet angles in shallow water are utilized, which were obtained from Jiang et al. [4] and Abessi and Roberts [13] (only their data for shallow water were used in the present study).

2. Gene expression programming

The GEP was developed by Ferreira [34] as a current extension of genetic programming (GP). GEP functions with a range of computer programs of varying sizes and shapes encoded in fixed-length linear chromosomes [29,35]. The chromosomes in a GEP algorithm are known as expression trees (ET). GEP utilizes genetic algorithm (GA) operators and is based on five elements: a terminal condition, control parameters, a fitness function, a terminal set and a function set.

To acquire the solution, a fixed-length chromosome string is employed to develop the GEP algorithm, while a parse tree structure is used in the GP structure over different periods of time for which the computer program is running. Due to the genetic mechanism of GEP at the chromosome level, the genetic diversity of such algorithm is extremely simple. Additionally, different complex nonlinear relations with various sub-programs can be built owing to the multi-genetic nature of GEP [36].

Each GEP gene utilizes two types of variables: fixed-length and constant. The constant variables in each gene are considered functional sets (FS), which can be arithmetic operations (e.g. {+, –, × , ÷ , exp, sin}) or terminal sets (TS) (e.g. {x_1, x_2, x_3, 5}). TS and FS must be defined to produce the chromosomes and genes [37,38]. One of the main features of GEP is chromosome production, where the chromosomes are represented by parse trees. Karva language developed by Ferreira [34] is used to read the information encoded in each chromosome.

The chromosomes are translated into different sub-expression trees (sub-ET). The transmutation of the expression translated by Karva into each ET begins from the first ET location in the expression (i.e. ET root) and continues in a left-to-right direction throughout the string. Owing to the predefined fixed length of GEP genes and variability of corresponding ET size, a number of inefficient extra components are present in the genome mapping procedure. As a result, the K-expression (Eq. 1) length can be equal to or less than the gene [39]. A common GEP program is as follows:

$$-.\times.+.-.x_1.-.\log.x_2.x_3.7.x_4.x_1 \tag{1}$$

where ''.'' is a component separator to simplify reading, "7" is a constant and x_1, x_2, x_3, x_4 are variables. The gene in Eq. (1) is expressed in Fig. 2. The sample gene in Eq. (1) is expressed in mathematical form in Eq. (2).

$$\left(\left(x_2-x_3\right)\times x_1\right)-\left(\left(7-x_4\right)+\log\left(x_1\right)\right) \tag{2}$$

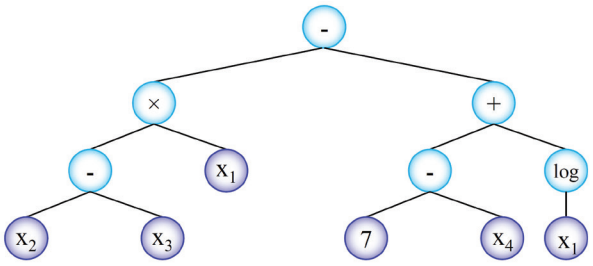

Fig. 2. Example ET.

A GEP algorithm employs the head-tail technique to guarantee the credibility of a randomly selected genome. GEP genes consist of heads and tails, where a tail includes TS and a head can be organized with both FS and TS [31,34].

A simple schematic of a GEP algorithm is given in Fig. 3. The GEP algorithm is initiated by randomly creating fixed-length chromosomes for each individual. Subsequently, the chromosomes are identified and the fitness of each individual is calculated. The chromosomes are selected based on their fitness, and the selected chromosomes are utilized to modify their reproduction. The same evolution process is repeated for new individuals in a series of generations until a solution is found or the specified number of generations is reached [34,39]. The best individuals are selected based on fitness, the roulette wheel selection method and elitism and are kept in the next generation [31]. Employing the single or multi-genetic operators, such as replication, transposition, recombination and mutation on the chosen chromosomes results in population variation to attain the best solution.

3. Methodology

Assuming fully turbulent flow where the Reynolds number ($R = uD/\nu$) is greater than 2,000, ν is the kinematic viscosity, the Boussinesq approximation is credible ($(\rho_0-\rho_a) \ll \rho_a$), and ρ_0 and ρ_a are the effluent and ambient density respectively. The variable dependent on flow (φ) is a function of momentum (M), ambient depth (H), discharge angle (θ), volume kinematic flux (Q) and buoyancy (B):

$$\phi = f\left(M,H,B,\theta,Q\right) \tag{3}$$

where

$$Q = \frac{\pi}{4}D^2u \tag{4}$$

$$B = g_0'Q \tag{5}$$

$$g_0' = g\left(\rho_0-\rho_a\right)/\rho_a \tag{6}$$

$$M = uQ \tag{7}$$

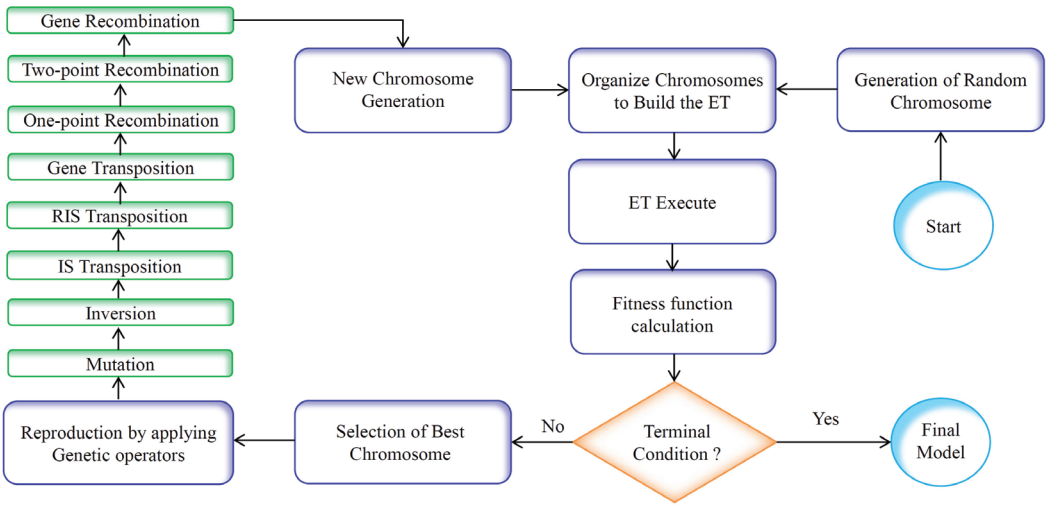

Fig. 3. Schematic presentation of a GEP algorithm.

where u is the jet's exit velocity. The most important length scale of flow that forms from buoyancy fluxes and momentum is $L_M = M^{3/4}/B^{1/2}$ [4,5,8,11,12], which is equal to $DF(\pi/4)^{1/4}$, where F is the jet's densimetric Froude number:

$$F = \frac{u}{\sqrt{Dg_0'}} \tag{8}$$

For high jet densimetric Froude number values ($F > 20$), the effect of the initial volume flux (Q) is not dynamically significant [5]. Then any variable dependent on shallow water flow depth can be written as:

$$\phi = f\left(M, H, B, \theta\right) \tag{9}$$

Therefore, the following dimensional analysis is presented in this study for non-dimensional horizontal displacement of the return point (x_r/D), non-dimensional horizontal displacement of the minimum surface dilution point (x_s/D), dilution at the return point (S_r) and minimum dilution at the water surface (S_S):

$$x_r / D = f\left(\theta, F, H / D\right) \tag{10}$$

$$x_S / D = f\left(\theta, F, H / D\right) \tag{11}$$

$$S_S = f\left(\theta, F, H / D\right) \tag{12}$$

$$S_r = f\left(\theta, F, H / D\right) \tag{13}$$

GEP is employed to present explicit equation for the previous dimensionless variables.

The data used in this study were collected from literature [4,13]. The data were measured experimentally by Jiang et al. [4] and Abessi and Roberts [13] for the non-dimensional horizontal displacement of the return point (x_r/D), non-dimensional horizontal displacement of the minimum surface dilution point (x_s/D), dilution at the return point (S_r) and minimum water surface dilution at the centerline maximum height (S_S) as follows: $5 < F < 82.5$, $15 < H/D < 79.44$ and $\theta = 30°$, 45° and 60°. 3D plots of all datasets are presented in Fig. 4.

4. GEP development for inclined dense jet prediction

In this study, GEP was developed using jEdit open-source software [40] to predict inclined dense jets. First, the "training set" and "testing set" were defined. K-fold cross validation was employed, whereby all samples were randomly divided into k sub-samples. A part of the sub-samples were considered the testing samples and k–1 sub-samples were employed for model training. This procedure was repeated k times, so that each sub-sample served as testing data at least once. In this research, k is equal to 4. The learning environment was defined by testing set selection. In GEP development, five major steps were considered. The first step was fitness function selection. Upon reviewing various fitness functions reported in different studies, the root relative squared error (RRSE) was chosen for the current study. RRSE is one of the most popular fitness functions utilized in recent research [29,32]. The fitness (f_i) of an individual program i is defined as follows:

$$f_i = \frac{1000}{1 + \mathrm{RRSE}_i} \tag{14}$$

Because RRSE_i is in the range of 0 and infinity, the fitness function value is in the [0 1000] range. RRSE_i is calculated as follows:

$$\mathrm{RRSE}_j = \sqrt{\frac{\sum_{i=1}^{n}\left(p_{ij} - O_i\right)^2}{\sum_{i=1}^{n}\left(O_i - \overline{O}\right)^2}} \tag{15}$$

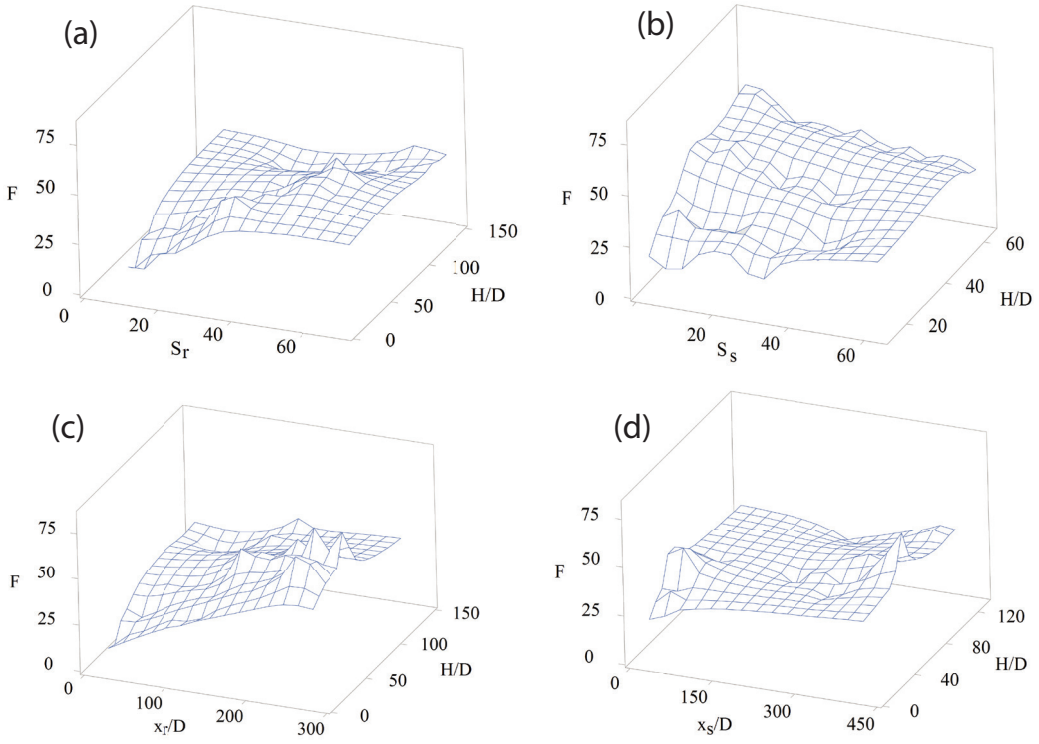

Fig. 4. 3D plots of datasets, (a) S_r, (b) S_s, (c) x_r/D and (d) x_s/D.

where O_i is the observed value, P_{ij} is the value predicted using program j for fitness i, n is the sample number, and $\bar{O}$ is the mean of all observed samples.

In the second step, the FS and TS were selected to generate the chromosomes. In this study, TS includes multi-independent variables as follows: $TS = \{\theta, F, H/D\}$. There is no specific way to select a suitable FS, but a good conjecture could be synergetic if it consists of all essential functions. Four arithmetic operators (+, ×, −, ÷) and some mathematical functions were applied in this study. To select these functions, basic mathematical functions such as log, √, etc. were used. Subsequently, the performance of one mathematical function combined with an arithmetic operator was evaluated. Then another function was added as an FS. If the function was efficient, it was considered in combination with new functions. This trial and error continued until the optimum FS was attained.

After selecting the TS and FS, the chromosome architecture was designed in the third step, including the number of genes, head lengths and number of chromosomes. The initial gene number, head length and chromosome number considered were 1, 2 and 30, respectively. These values were increased one at a time through each run and GEP performance was monitored in training and testing. The results indicate that more than three genes, a chromosome number greater than 200 or 400 for some models and head length over 20 or 30 for some models did not significantly improve GEP performance in training and testing.

In the fourth step, four linking functions were examined: addition, subtraction, multiplication and division. The results indicate the superior performance of addition over the other linking functions. The final step entailed selecting genetic operators that create diversity. The optimum values of each parameter are presented in Table 1.

5. Results and discussion

This section presents the GEP modeling results. Root mean square error (RMSE), root relative squared error (RRSE), mean absolute percentage error (MAPE), BIAS and correlation coefficient (R) are utilized to demonstrate the prediction errors. These error indices are defined as follows:

$$\mathrm{RMSE} = \sqrt{\frac{1}{n}\sum_{i=1}^{n}\left(P_i - O_i\right)^2} \tag{16}$$

$$\mathrm{RRSE} = \sqrt{\frac{\sum_{i=1}^{n}\left(P_i - O_i\right)^2}{\sum_{i=1}^{n}\left(O_i - \overline{O}\right)^2}} \tag{17}$$

$$\mathrm{MAPE} = \sum_{i=1}^{n}\frac{100\times\left(P_i - O_i\right)}{P_i} \tag{18}$$

$$R = \left(\frac{\sum_{i=1}^{n}\left(P_i - \bar{P}\right)\left(O_i - \bar{O}\right)}{\sqrt{\sum_{i=1}^{n}\left(P_i - \bar{P}\right)^2\sum_{i=1}^{n}\left(O_i - \bar{O}\right)^2}}\right) \tag{19}$$

Table 1
Optimum parameter settings for GEP modeling

	Parameters	S_r	S_S	X_r/D	X_S/D
P1	Number of generations	5,00,000	5,00,000	5,00,000	5,00,000
P2	Number of chromosomes	200	200	400	400
P3	Number of genes	3	3	3	3
P4	Head size	10	20	30	30
P5	Linking function	Addition	Addition	Addition	Addition
P6	Type of fitness function	RRSE	RRSE	RRSE	RRSE
P7	Mutation rate	0.014	0.014	0.04	0.014
P8	Inversion rate	0.15	0.1	0.15	0.1
P9	IS transposition	0.15	0.1	0.15	0.1
P10	RIS transposition	0.15	0.1	0.15	0.1
P11	One-point recombination rate	0.35	0.3	0.35	0.4
P12	Two-point recombination rate	0.35	0.3	0.35	0.4
P13	Gene recombination rate	0.15	0.15	0.15	0.15
P14	Gene transportation rate	0.15	0.15	0.15	0.15
P15	Function set	+, ×, –, ÷, Log, X_2, 3Rt	+, ×, –, ÷, sinh, Asinh, cosh, cos, Tan, Atanh, sqrt, 3Rt, 4Rt, 5Rt, Log, Exp	+, ×, –, ÷, cosh, Tan, Cos, 4Rt, Exp, sqrt, Log, 3Rt, Asinh, sinh, X_3, sin	+, ×, –, ÷, Asinh, sin, Acosh, cos, cosh, Acos, Tan, Tanh, Log, Exp, 3Rt, 4Rt, 5Rt, X_2, X_3

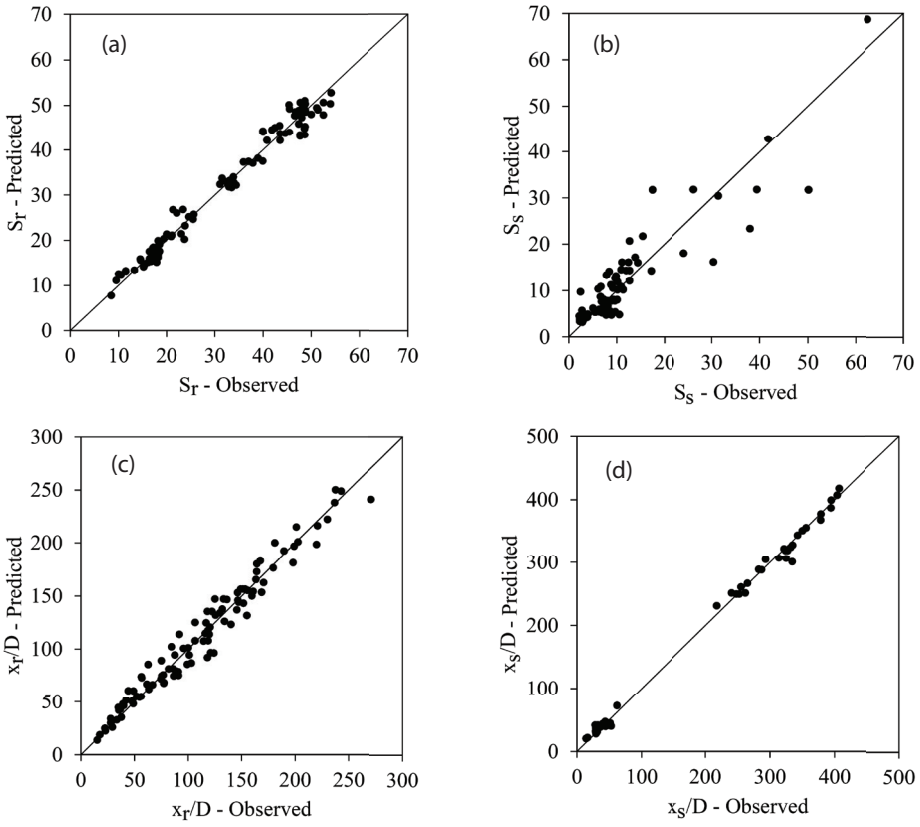

Fig. 5. Scatter plots of GEP predictions of (a) S_r, (b) S_S, (c) x_r/D and (d) x_S/D.

$$\text{BAIS} = \frac{\sum_{i=1}^{n}(P_i - O_i)}{n} \quad (20)$$

where O_i is the observed value, P_i is the predicted value, n is the number of samples, and $\bar{O}$ is the mean of all observed samples.

Fig. 5 presents scatter plots of the GEP predictions of S_r, S_S, x_r/D and x_S/D (see Appendix A for more details). The GEP prediction results of dilution at the return point (S_r) were highly accurate, as most samples predicted by GEP are near the best-fit line. According to Table 2, the correlation coefficient for this model was 0.989. The mean absolute percentage error (MAPE) presented 6% error in S_r prediction. The RMSE and RRSE absolute and relative values were 2.078 and 0.149 respectively, indicating the high ability of GEP in S_r prediction. BIAS of –0.004 demonstrates model underestimation. However, this index value was insignificant relative to the S_r values.

S_s prediction by GEP was weaker than that of S_r. According to Fig. 5, the GEP-based equation for S_S prediction produced appropriate results for $S_S < 20$, beyond which, the model performance deteriorated with MAPE of 34%. The general performance of GEP in S_S prediction was surveyed in terms of the BIAS index. The positive value (BIAS = 0.229) demonstrates GEP model overestimation.

The GEP prediction results for the dimensionless horizontal displacement of the return point (x_r/D) and non-dimensional horizontal displacement of the minimum surface dilution point (x_s/D) indicate high modeling accuracy. A qualitative examination of the models signifies that all models with these variables (x_s/D and x_r/D) are near the best-fit line. Therefore, GEP is a good means of predicting these variables. Moreover, a quantitative survey (Table 2) indicates that the relative errors for x_s/D and x_r/D prediction were 8.217 and 9.328, respectively. The root mean error indices (RMSE and RRSE) were 8.033 and 0.055 (x_s/D) and 11.256 and 0.19 (x_r/D). The x_s/D and x_r/D prediction trends were underestimation and overestimation, respectively. Based on the results in Fig. 5 and Table 2, it can be concluded that GEP is an evolutionary tool highly capable of predicting horizontal jet displacement and dilution in shallow water.

The variation trend of S_r, S_S, x_r/D and x_S/D in relation to the input variables was analyzed by partial derivative sensitivity analysis (PDSA) [31,41]. The sensitivity of each input variable x_i on the target variable was surveyed using the partial derivative of the target value (K) to each input (x_i), (dK/dx_i). A positive (or negative) PDSA value implies that an increase in x_i as ε ($x_i + \varepsilon$) leads to an increase (or decrease) in K. Fig. 6 displays the sensitivity analysis results for different input variables in S_r prediction. The figure signifies the S_r values do not follow a certain trend with the increase or decrease in H/D value, as the sensitivity values in each H/D

Table 2
Statistical indices for GEP predictions of S_r, S_S, x_r/D and x_S/D

Variable	R	MAPE	RMSE	RRSE	BIAS
Perfect value	1	0	0	0	0
S_S	0.909	34.002	4.555	0.419	0.229
S_r	0.989	6.013	2.085	0.149	–0.004
x_s/D	0.999	8.217	8.033	0.055	–0.074
x_r/D	0.982	9.328	11.256	0.190	0.458

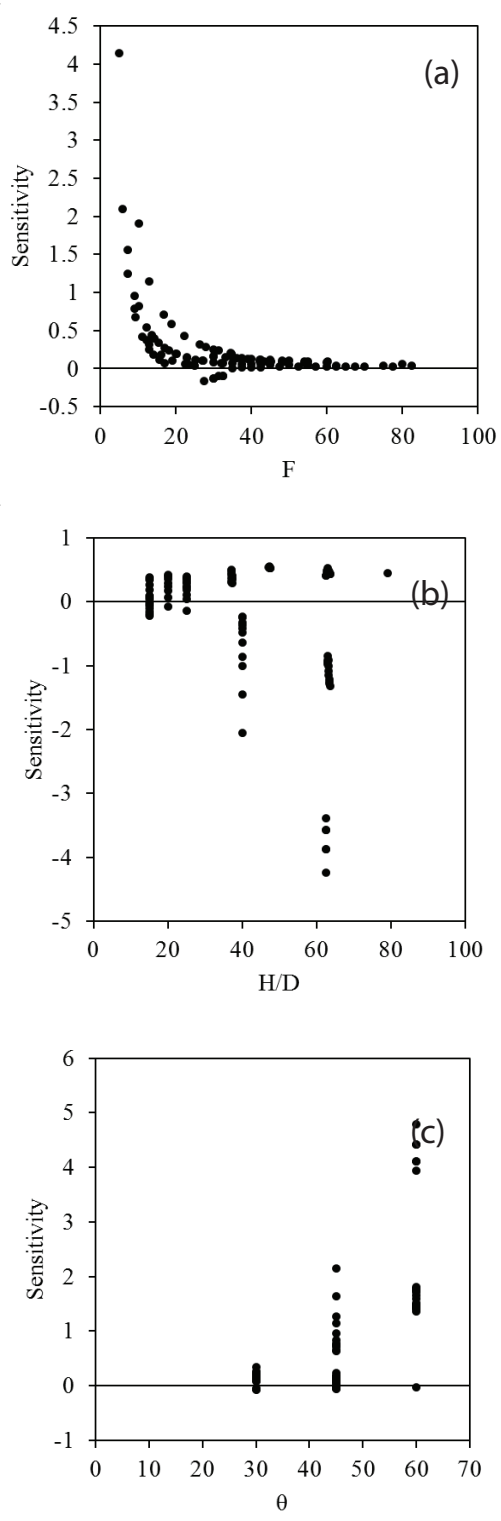

Fig. 6. Sensitivity analysis results for different input variables in S_r prediction, (a) F, (b) H/D and (c) θ.

range were positive and negative. The increase or decrease in H/D at lower H/D values had a lower impact on S_r compared with an increase or decrease in higher H/D values. The PDSA values for 30°, 45° and 60° indicate that an increase in θ value resulted in an increase in S_r value, whereby sensitivity increased with increasing θ. It should be noted that the sensitivity reduced with increasing F.

Fig. 7 shows the sensitivity analysis results for different input variables in S_S prediction. The increase or decrease in the F variable in S_S prediction led to a significant increase or decrease in Ss, with PDSA values between -10^3 and 10^3. Therefore, the GEP-based equation presented for S_S prediction is very sensitive to F and any insignificant change in this variable resulted in a significant change in S_S. Most PDSA results of the proposed model's sensitivity to H/D were negative. Then an increase in H/D led to a lower S_S calculated by the GEP-based model. Moreover, the GEP-based model's sensitivity to θ did not exhibit a certain trend, as various positive and negative PDSA values were obtained for different ranges of this variable. The sensitivity analysis results indicate the lowest sensitivity of the GEP-based model to θ compared with F and H/D.

Fig. 8 presents the sensitivity analysis results for different input variables in x_r/D prediction. The PDSA results indicate that a change in the H/D and θ parameters influencing x_r/D prediction exhibited no deterministic trend in x_r/D values, as the PDSA values were negative or positive in different ranges. It should be noted that the PDSA values were relatively low, signifying the low sensitivity of the proposed model to these variables. In contrast to these two parameters, the sensitivity of the proposed model to F was second-order, as with increasing toward maximum F, the sensitivity values changed from positive to negative.

The sensitivity analysis results for different input variables in x_S/D prediction show there was no certain trend in the PDSA analysis to conclude that any changes in these parameters (θ, F or H/D) while other parameters (two of three input variables) remained constant resulted in an increase or decrease in the target value (x_S/D). However, the PDSA values relative to all input variables indicate that any change in these parameters often had significant impact on the x_S/D values.

A quantitative appraisal of the uncertainties in S_r, S_S, x_r/D and x_S/D prediction is presented in Table 3. Uncertainty analysis was applied to the test data utilized in this research [42–43]. The prediction error $e_j = P_j - O_j$ can be described with uncertainty analysis. The prediction errors computed for the entire dataset were applied to compute the standard deviation and mean prediction errors $S_e = \sqrt{\sum_{j=1}^{n}\left(e_j - \bar{e}\right)^2 / \left(n-1\right)}$ and $\bar{e} = \sum_{j=1}^{n} e_j / n$, respectively. Positive and negative mean values demonstrate prediction model overestimation and underestimation, respectively. An uncertainty bound was defined for mean prediction error and S_e by Wilson score technique without continuity correction. The use of ± 1.98 S_e yielded an approximately 95% uncertainty band. The uncertainty analysis results for the S_r, S_S, x_r/D and x_S/D variables are presented in Table 3. This table also shows the mean prediction error, uncertainty band width and 95% prediction error interval. The results indicate that the absolute mean prediction errors for the GEP developed to predict S_r, S_S, x_r/D and x_S/D were 0.004, –0.229, –0.458 and 0.051 respectively. The widths of the uncertainty bounds were ± 0.418, ± 1.012, ± 2.209 and ± 1.473 for S_r, S_S, x_r/D and x_S/D.

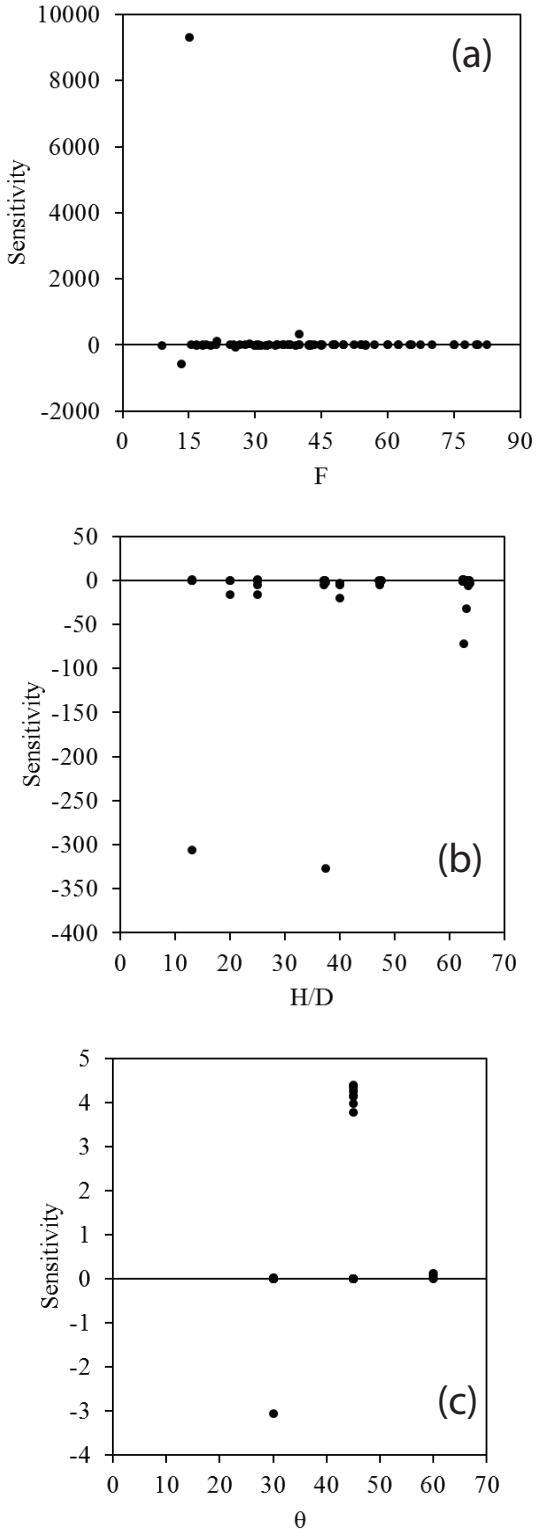

Fig. 7. Sensitivity analysis results for different input variables in S_S prediction, (a) F, (b) H/D and (c) θ.

Table 3
Uncertainty analysis of the GEP models developed

Model	# of samples	Mean value	Mean prediction error	Uncertainty interval half width	95% prediction error interval
x_r/D	103	175.46	–0.458	± 2.209	(–2.667 1.750)
S_r	99	0.004	0.004	± 0.418	(–0.414 0.422)
S_S	81	31.42	–0.229	± 1.012	(–1.242 0.783)
x_s/D	55	111.92	0.051	± 1.473	(–1.422 1.523)

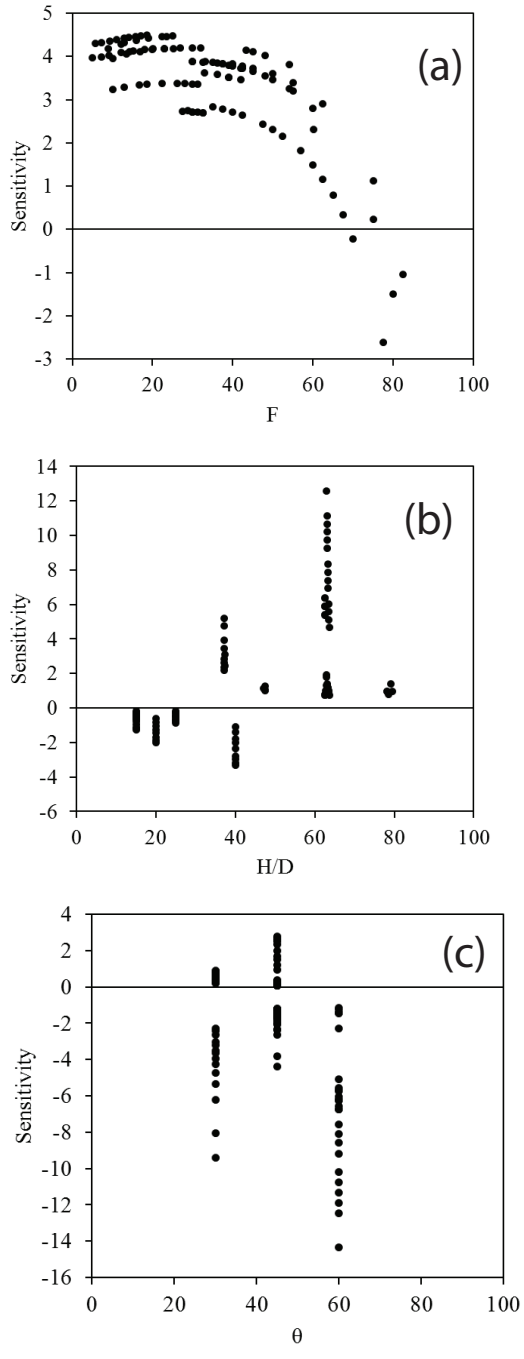

Fig. 8. Sensitivity analysis results for different input variables in x_r/D prediction, (a) F, (b) H/D and (c) θ.

6. Conclusions

This study presented the application of the GEP technique to develop a model for predicting the characteristics of an inclined dense jet in shallow water (inclined dense jet impacts the water surface), i.e. the non-dimensional horizontal displacement of the return point (x_r/D), non-dimensional horizontal displacement of the minimum surface dilution point (x_s/D), dilution at the return point (S_r) and minimum dilution at the water surface (S_S). The GEP technique was introduced to attain the global minimum through an evolutionary process. Four pseudocodes were presented to calculate x_r/D, x_s/D, S_r and S_S. The results of the proposed models displayed high accuracy in predicting x_r/D (R = 0.982; MAPE = 9.328; RRSE = 0.190), x_s/D (= 0.999; MAPE = 8.217; RRSE = 0.055), S_r (R = 0.989; MAPE = 6.013; RRSE = 0.149) and S_S (R = 0.909; MAPE = 34.002; RRSE = 0.419). Partial derivative sensitivity analysis was also conducted to survey the effect of each input variable. According to the results, x_r/D is highly sensitive to non-dimensional ambient depth (H/D) and discharge angle (θ), S_s is highly sensitive to the jet densimetric Froude number (F) and S_r and x_s/D are sensitive to all input variables (F, θ and H/D). Moreover, uncertainty analysis was conducted and the uncertainty band widths identified for S_r, S_s, x_r/D and x_s/D were ± 0.418, ± 1.012, ± 2.209 and ± 1.473 respectively. Therefore, the GEP models developed in this paper can serve as suitable alternatives in practical engineering problems.

Acknowledgment

The project was supported by the Natural Sciences and Engineering Research Council of Canada (NSERC).

References

[1] A.B. Pincince, E.J. List, Disposal of brine into an estuary, J. Water. Pollut. Control. Fed., 45 (1973) 2335–2344.
[2] S.J. Yoon, G.S. Park, Ecotoxicological effects of brine discharge on marine community by seawater desalination, Desal. Wat. Treat., 33 (2011) 240–247.
[3] R. Einav, K. Harussi, H. Perry, The footprint of the desalination processes on the environment, Desalination, 152 (2003) 141–154.
[4] B. Jiang, A.W.K. Law, J.H.W. Lee, Mixing of 30 and 45 inclined dense jets in shallow coastal waters, J. Hydraul. Eng., 140 (2014) 241–253.
[5] P.J.W. Roberts, A. Ferrier, G.J. Daviero, Mixing in inclined dense jets, J. Hydraul. Eng., 123 (1997) 693–699.
[6] M.A. Zeitoun, W.F. McHilhenny, R.O. Reid, Conceptual designs of outfall systems for desalination plants, Research and Development Progress. Washington D.C., Office of Saline Water. United States Department of the Interior. USA, 1970.
[7] P.J.W. Roberts, G. Toms, Inclined dense jets in flowing current, J. Hydraul. Eng., 113 (1987) 323–341.

[8] G.H. Jirka, Integral model for turbulent buoyant jets in unbounded stratified flows. Part I: single round jet, Environ. Fluid. Mech., 4 (2004) 1–56.
[9] A. Cipollina, A. Brucato, F. Grisafi, S. Nicosia, Bench-scale investigation of inclined dense jets, J. Hydraul. Eng., 131 (2005) 1017–1022.
[10] G.A. Kikkert, M.J. Davidson, R.I. Nokes, Inclined negatively buoyant discharges, J. Hydraul. Eng., 133 (2007) 545–554.
[11] D. Shao, A.W.K. Law, Mixing and boundary interactions of 30° and 45° inclined dense jets, Environ. Fluid. Mech., 10 (2010) 521–553.
[12] C. Lai, J.H.W. Lee, Mixing of inclined dense jets in stationary ambient, J. Hydro-Environ. Res., 6 (2012) 9–28.
[13] O. Abessi, P.J. Roberts, Dense jet discharges in shallow water, J. Hydraul. Eng., 142 (2016) 04015033.
[14] R. Bashitialshaaer, M. Larson, K.M. Persson, An experimental investigation on inclined negatively buoyant jets, Water: Adv. Water. Desal., 4 (2012) 720–738.
[15] A.Cipollina, A. Bonfiglio, G. Micale, A. Brucato, Dense jet modelling applied to the design of dense effluent diffusers, Desalination, 167 (2004) 459–468.
[16] A. Cipollina, A. Bonfiglio, G. Micale, A mathematical tool for describing the behaviour of a dense effluent discharge, Desal. Wat. Treat., 2 (2009) 303–318.
[17] I.K. Nikiforakis, A.I. Stamou, G.C.A. Christodoulou, Modified integral model for negatively buoyant jets in a stationary ambient, Environ. Fluid. Mech., 15 (2015) 939–957.
[18] G.A. Kikkert, M.J. Davidson, R.I. Nokes, Buoyant jets with three-dimensional trajectories, J. Hydraul. Res., 48 (2010) 292–301.
[19] P. Vafeiadou, I. Papakonstantis, G. Christodoulou, Numerical simulation of inclined negatively buoyant jets, The 9th international conference on environmental science and technology, September, Rhodes Island, Greece, 2005, pp. 1–3.
[20] D.G. Kim, H.Y. Cho, Modeling the buoyant flow of heated water discharged from surface and submerged side outfalls in shallow and deep water with a cross flow, J. Environ. Fluid. Mech., 6 (2006) 501–518.
[21] C.J. Oliver, M.J. Davidson, R.I. Nokes, k-ε Prediction of the initial mixing of desalination discharges, J. Environ. Fluid. Mech., 8 (2008) 617–625.
[22] H. Kheirkhah Gildeh, A. Mohammadian, I. Nistor, H. Qiblawey, Numerical modeling of turbulent buoyant wall jets in stationary ambient water, J. Hydraul. Eng., 140 (2014) 04014012.
[23] S. Zhang, A.W.K. Law, M. Jiang, Large eddy simulations of 45 and 60 inclined dense jets with bottom impact, J. Hydro-Environ. Res., 15 (2017) 54–66.
[24] P. Angelidis, D. Kalpakis, V. Gyrikis, N. Kotsovinos, 2D brine sewage after impinging on a shallow sea free surface, J. Environ. Fluid. Mech., 17 (2017) 615–628.
[25] H. Kheirkhah Gildeh, A. Mohammadian, I. Nistor, H. Qiblawey, Numerical modeling of 30° and 45° inclined dense turbulent jets in stationary ambient, J. Environ. Fluid. Mech., 15 (2015) 537–562.
[26] D. Robinson, M. Wood, M. Piggott, G. Gorma, CFD modelling of marine discharge mixing and dispersion, J. Appl. Water. Eng. Res., 4 (2016) 152–162.
[27] P. Palomar, J.L. Lara, I.J. Losada, L. Tarrade, Numerical modeling of brine discharge: commercial models, MEDVSA online simulation tools and advanced computational fluid dynamics, Desal. Wat. Treat., 51 (2013) 543–559.
[28] H.M. Azamathulla, Gene expression programming for prediction of scour depth downstream of sills, J. Hydrol., 460 (2012) 156–159.
[29] I. Ebtehaj, H. Bonakdari, A.H. Zaji, H. Azimi, A. Sharifi, Gene expression programming to predict the discharge coefficient in rectangular side weirs, Appl. Soft. Comput., 35 (2015) 618–628.
[30] A. Gholami, H. Bonakdari, A.H. Zaji, A.A Akhtari, S.R. Khodashenas, Predicting the velocity field in a 90° open channel bend using a gene expression programming model, Flow. Meas. Instrum., 46 (2015) 189–192.
[31] H. Azimi, H. Bonakdari, I. Ebtehaj, A highly efficient gene expression programming model for predicting discharge coefficient in a side weir along a trapezoidal canal, Irrig. Drain., 66 (2017) 655–666.
[32] Z.S. Khozani, H. Bonakdari, I. Ebtehaj, An analysis of shear stress distribution in circular channels with sediment deposition based on gene expression programming, Int. J. Sediment. Res., (2017) 575–584.
[33] D.A. Botelho, B. Miller, P. Roberts, O. Obessi, M. Mohammadian, M. Wood, D.D. Shao, J. Bradley, R. Morelissen, A.W.K. Law, Marine Outfall Systems: Current Trends, Research and Challenges. In H. Li (Ed.), Global Trends & Challenges in Water Science, Research and Management: a compendium of hot topics and features from IWA specialist groups (2 ed., pp. 67–72). London, UK, 2016.
[34] C. Ferreira, Gene expression programming: a new adaptive algorithm for solving problems, Complex. Syst., 13 (2001) 87–129.
[35] C. Ferreira, Gene Expression Programming. Mathematical modeling by an artificial intelligence. 2nd ed. Germany: Springer-Verlag Publication, 2006.
[36] H. Moeeni, H. Bonakdari, I. Ebtehaj, Monthly reservoir inflow forecasting using a new hybrid SARIMA genetic programming approach, J. Earth. Syst. Sci., 126 (2017) 1–13.
[37] A.H. Gandomi, S.K. Babanajad, A.H. Alavi, Y.A. Farnam, Novel approach to strength modeling of concrete under triaxial compression, J. Mater. Civ. Eng., 24 (2012) 1132–1143.
[38] A.H. Alavi, A.H. Gandomi, A robust data mining approach for formulation of geotechnical engineering systems, Eng. Comput., 28 (2011) 242–274.
[39] I. Ebtehaj, H. Bonakdari, Comparison of genetic algorithm and imperialist competitive algorithms in predicting bed load transport in clean pipe, Water. Sci. Technol., 70 (2014) 1695–1701.
[40] JEdit. (2011). http://sourceforge.net/projects/jedit/.
[41] I. Ebtehaj, H. Bonakdari, A.H. Zaji, H. Azimi, F. Khoshbin, GMDH-type neural network approach for modeling the discharge coefficient of rectangular sharp-crested side weirs, Eng. Sci. Technol., Int. J., 18 (2015) 746–757.
[42] A.M. Sattar, B. Gharabaghi, E. McBean, Predicting timing of watermain failure using gene expression models for infrastructure planning, Water Resour. Manage., 30 (2016) 1635–1651.
[43] I. Ebtehaj, A.M. Sattar, H. Bonakdari, A.H. Zaji, Prediction of scour depth around bridge piers using self-adaptive extreme learning machine, J. Hydroinformatics., 19 (2017) 207–224.

Appendix A

The GEP output is an enforceable equation. The equations extracted for S_S, S_r, x_S/D, x_r/D are given in Table A1.

Table A1
GEP-based equations related to S_S, S_r, x_S/D, x_r/D

Variable	Equation	Eq. No.
S_r	$S_r = S_r(1) + S_r(2) + S_r(3)$	A1
	$S_1(1) = (((\theta/(F\text{-}3.09)) + ((F/3.09) + \theta))/((\text{-}0.09 \times F) \times (\theta\text{-}H/D)))$	A2
	$S_r(2) = (\theta/((((1.3 \times (H/D)) + F)/4.82) - (\log(F) - ((H/D)/F))))$	A3
	$S_r(3) = (((\log(((((H/D)/\theta) \times (H/D + 4.73)) + \log(F))) \times (H/D))\text{^}(1/3))\text{^}2)$	A4
S_S	$S_S = S_S(1) + S_S(2) + S_S(3)$	A5
	$S_S(1) = \sinh(\sinh(((\cosh(\text{asinh}(H/D)) - \tan(((H/D/(((\cos((\text{-}4.41+F)) + (H/D\text{^}(0.2))) + 1.83)\text{^}(0.25)))+F)))/F)))$	A6
	$S_S(2) = (\text{H/D*}(1/(1 + \exp(\text{-}(((\text{sqrt}(((1/(1 + \exp(\text{-}(H/D\text{-}25.33))))\text{^}(0.2))) + \log(H/D))\text{-}\theta)+\sinh(\tan((6.75*F))))))))$	A7
	$S_S(3) = \sinh(\text{sqrt}((\exp(((H/D*(\text{asinh}(H/D)/\text{atanh}(\exp(\text{-}((1/(1 + \exp(\text{-}(\theta\text{-}4.45\text{-}H/D+\theta/F))) + 1/(1+\exp(\text{-}(\text{-}3.57))))\text{^}2)))))\text{^}(1/3)))\text{^}(1/3))))$	A8
x_S/D	$x_s / D = x_s / D(1) + x_s / D(2) + x_s / D(3)$	A9
	$x_s/D(1) = (F \times \text{asinh}(((\sin(\log(\text{acosh}((\text{asinh}(\cos(\exp((F + \exp((((\text{acos}((0.48 \times (((\exp(\text{-}((F\text{-}3.14)\text{^}2)))\text{^}(0.2)) + \cos((\text{-}3.14 + \theta)))))\text{^}(1/3))+0.48)\text{^}2))))))+F))))\times(H/D))\text{-}\theta)))$	A10
	$x_s/D(2) = (((\cos(H/D) \times ((\tan((\tanh(9.21) + \tan(F))) + \tan((9.21. \times (H/D)))) + (F + ((((H/D)\text{^}2) - (H/D.\times 9.21))\text{^}(0.25))))) + ((H/D + \sin(((\text{-}8.19\text{-}F) - (F\text{-}H/D)))) + 8.19)) + F)$	A11
	$x_s/D(3) = F + (F + (\log10((((7.84/H/D) \times \sinh((\text{atanh}((\cos(\cosh(((H/D)\text{^}(1/3)))) \times (1/(1 + \exp(\text{-}(\sin((H/D+F)) + (F\text{-}H/D) + F))))))\text{^}2)))\text{^}3)) \times \cos(((\log10(F) + F) \times \theta)))))$	A12
x_r/D	$x_r / D = x_r / D(1) + x_r / D(2) + x_r / D(3)$	A13
	$x_rD(1) = ((\log((F + ((F\text{^}(1/3))\text{^}2))) \times (\text{sqrt}((F/\theta))\text{^}(1/3)))\text{^}3)$	A14
	$x_rD(2) = (\log((((((\theta\text{-}H/D)\text{^}2) \times \theta)/(H/D))\text{^}(1/4)))\times F)$	A15
	$x_rD(3) = (F\text{-}((((\exp(F)\text{^}(1/4)) \times ((\theta/3.78) \times \theta))\text{^}(1/3))/F))$	A16

The results of the GEP-based equations in predicting S_S, x_S/D, S_r, x_r/D are presented in Tables A2 to A5, respectively.

Table A2
GEP results for S_S prediction

Reference	θ	F	H/D	S_s–Actual	S_s–GEP
Jiang et al. [4]	30	21.4	20	31.3	30.48
Jiang et al. [4]	30	26.5	20	9.52	7.81
Jiang et al. [4]	30	34.6	20	6.58	8.74
Jiang et al. [4]	30	30.8	20	7.84	7.80
Jiang et al. [4]	30	38	20	6.76	7.71
Jiang et al. [4]	30	13.4	13	30.3	16.23
Jiang et al. [4]	30	15.1	13	10.9	10.89
Jiang et al. [4]	30	16.7	13	8.44	5.64
Jiang et al. [4]	30	18.9	13	6.15	5.51
Jiang et al. [4]	30	21.1	13	5.62	5.46
Jiang et al. [4]	30	24.4	13	5.56	5.39
Jiang et al. [4]	45	25.5	40	37.9	23.42
Jiang et al. [4]	45	27.8	40	24.1	18.06
Jiang et al. [4]	45	30.7	40	13.8	17.15
Jiang et al. [4]	45	36.6	40	10.9	14.49
Jiang et al. [4]	45	44.7	40	9.81	13.17
Jiang et al. [4]	45	48	40	9.61	12.74
Jiang et al. [4]	45	65.5	40	8.76	11.27
Jiang et al. [4]	45	80.5	40	9.13	10.57
Jiang et al. [4]	45	15.6	25	41.7	42.88
Jiang et al. [4]	45	16.7	25	17.2	14.30
Jiang et al. [4]	45	18.1	25	10.1	11.94
Jiang et al. [4]	45	20	25	8.4	14.10
Jiang et al. [4]	45	25.2	25	6.67	10.85
Jiang et al. [4]	45	30.4	25	6.06	10.39
Jiang et al. [4]	45	9	13	6.67	8.66
Jiang et al. [4]	45	18.1	13	2.67	5.73
Abessi and Roberts [13]	30	42.1	47.30	3.79	4.26
Abessi and Roberts [13]	30	43.3	47.58	3.90	4.90
Abessi and Roberts [13]	30	45.1	47.47	3.61	4.87
Abessi and Roberts [13]	30	48.1	47.16	3.37	4.49
Abessi and Roberts [13]	30	54.1	47.46	3.25	4.25

(*Continued*)

Table A2 (*Continued*)

Reference	θ	F	H/D	S_s–Actual	S_s–GEP
Abessi and Roberts [13]	30	32.5	37.36	2.93	4.21
Abessi and Roberts [13]	30	35	37.23	3.15	4.43
Abessi and Roberts [13]	30	37.5	37.13	2.25	4.07
Abessi and Roberts [13]	30	40	37.38	2.40	9.80
Abessi and Roberts [13]	30	42.5	37.28	2.13	4.53
Abessi and Roberts [13]	30	45	37.19	2.25	3.82
Abessi and Roberts [13]	30	50	37.31	3.00	3.68
Abessi and Roberts [13]	30	55	37.16	2.75	3.20
Abessi and Roberts [13]	30	62.5	37.20	2.50	3.50
Abessi and Roberts [13]	30	75	37.13	2.25	3.38
Abessi and Roberts [13]	30	82.5	37.16	2.48	3.33
Abessi and Roberts [13]	45	30	62.50	17.40	31.77
Abessi and Roberts [13]	45	33.1	63.65	12.58	20.71
Abessi and Roberts [13]	45	36.1	63.33	12.64	12.18
Abessi and Roberts [13]	45	39.1	63.06	7.82	13.43
Abessi and Roberts [13]	45	42.1	62.84	7.16	8.16
Abessi and Roberts [13]	45	48.1	63.29	7.22	6.64
Abessi and Roberts [13]	45	54.1	62.91	7.57	5.91
Abessi and Roberts [13]	45	30	62.50	50.10	31.77
Abessi and Roberts [13]	45	32.5	62.50	14.30	16.02
Abessi and Roberts [13]	45	35	63.64	12.60	14.36
Abessi and Roberts [13]	45	37.5	63.56	11.25	10.26
Abessi and Roberts [13]	45	40	63.49	10.00	8.05
Abessi and Roberts [13]	45	42.5	63.43	8.93	7.84
Abessi and Roberts [13]	45	45	63.38	6.30	5.96

(*Continued*)

Table A2 (*Continued*)

Reference	θ	*F*	*H/D*	S_s–Actual	S_s–GEP
Abessi and Roberts [13]	45	50	63.29	5.00	6.20
Abessi and Roberts [13]	45	55	63.22	7.70	5.73
Abessi and Roberts [13]	45	60	63.16	5.40	5.43
Abessi and Roberts [13]	45	75	63.03	10.50	4.85
Abessi and Roberts [13]	45	80	62.99	8.80	4.76
Abessi and Roberts [13]	60	30	62.50	26.10	31.88
Abessi and Roberts [13]	60	32.5	62.50	11.05	16.12
Abessi and Roberts [13]	60	30	62.50	39.30	31.88
Abessi and Roberts [13]	60	32.5	62.50	12.35	16.12
Abessi and Roberts [13]	60	35	63.64	11.90	14.39
Abessi and Roberts [13]	60	37.5	63.56	10.13	10.29
Abessi and Roberts [13]	60	40	63.49	9.20	8.08
Abessi and Roberts [13]	60	42.5	63.43	8.08	7.87
Abessi and Roberts [13]	60	47.5	63.33	8.08	6.74
Abessi and Roberts [13]	60	52.5	63.25	7.88	5.76
Abessi and Roberts [13]	60	57	63.33	7.98	5.60
Abessi and Roberts [13]	60	62.5	63.13	6.88	5.28
Abessi and Roberts [13]	60	67.5	63.08	7.43	5.09
Abessi and Roberts [13]	60	28.8	62.61	62.50	68.71
Abessi and Roberts [13]	60	31.3	62.60	15.34	21.81
Abessi and Roberts [13]	60	60	63.16	9.60	5.45
Abessi and Roberts [13]	60	65	63.11	8.45	5.07
Abessi and Roberts [13]	60	70	63.06	7.70	4.95
Abessi and Roberts [13]	60	77.5	63.01	7.75	4.74

Table A3
GEP results for x_s/D prediction

Reference	θ	*F*	*H/D*	x_s/D–Actual	x_s/D–GEP
Jiang et al. [4]	30	21.4	20	46.1	41.18
Jiang et al. [4]	30	26.5	20	47.5	40.92
Jiang et al. [4]	30	34.6	20	43.7	47.05
Jiang et al. [4]	30	30.8	20	44.1	39.58
Jiang et al. [4]	30	38	20	42	40.08
Jiang et al. [4]	30	13.4	13	29.2	27.95
Jiang et al. [4]	30	15.1	13	30.1	29.31
Jiang et al. [4]	30	16.7	13	31.4	31.03
Jiang et al. [4]	30	18.9	13	30.1	32.02
Jiang et al. [4]	30	21.1	13	29.8	29.77
Jiang et al. [4]	30	24.4	13	28.8	31.55
Jiang et al. [4]	45	25.5	40	52.6	40.12
Jiang et al. [4]	45	27.8	40	49.9	44.44
Jiang et al. [4]	45	30.7	40	51.3	44.56
Jiang et al. [4]	45	36.6	40	49	44.81
Jiang et al. [4]	45	44.7	40	40	43.86
Jiang et al. [4]	45	48	40	40.9	41.86
Jiang et al. [4]	45	65.5	40	36.4	38.67
Jiang et al. [4]	45	80.5	40	35.8	38.76
Jiang et al. [4]	45	15.6	25	32.2	41.40
Jiang et al. [4]	45	16.7	25	31.5	36.66
Jiang et al. [4]	45	18.1	25	31.4	36.30
Jiang et al. [4]	45	20	25	32.5	35.50
Jiang et al. [4]	45	25.2	25	29.1	36.72
Jiang et al. [4]	45	30.4	25	28.2	41.55
Jiang et al. [4]	45	9	13	16.4	21.64
Jiang et al. [4]	45	18.1	13	14.1	20.29
Abessi and Roberts [13]	30	32.5	37.36	321.75	322.26
Abessi and Roberts [13]	45	30	62.50	327.00	319.56
Abessi and Roberts [13]	45	33.1	63.65	334.31	301.07
Abessi and Roberts [13]	45	36.1	63.33	342.59	343.96
Abessi and Roberts [13]	45	30	62.50	324.00	319.56
Abessi and Roberts [13]	45	32.5	62.50	334.75	328.24
Abessi and Roberts [13]	45	37.5	63.56	349.88	351.06

(*Continued*)

Table A3 (*Continued*)

Reference	θ	*F*	*H/D*	x_s/D–Actual	x_s/D–GEP
Abessi and Roberts [13]	45	40	63.49	378.40	368.31
Abessi and Roberts [13]	45	42.5	63.43	393.98	387.18
Abessi and Roberts [13]	45	45	63.38	403.65	407.44
Abessi and Roberts [13]	60	33	78.57	282.48	288.71
Abessi and Roberts [13]	60	36.1	78.48	293.13	304.65
Abessi and Roberts [13]	60	39.1	78.20	324.92	306.57
Abessi and Roberts [13]	60	27.5	62.50	217.53	231.08
Abessi and Roberts [13]	60	30	62.50	247.80	249.77
Abessi and Roberts [13]	60	32.5	62.50	261.63	251.41
Abessi and Roberts [13]	60	30	62.50	252.30	249.77
Abessi and Roberts [13]	60	32.5	62.50	240.50	251.41
Abessi and Roberts [13]	60	35	63.64	264.95	266.78
Abessi and Roberts [13]	60	37.5	63.56	286.88	288.22
Abessi and Roberts [13]	60	40	63.49	313.60	307.01
Abessi and Roberts [13]	60	42.5	63.43	331.93	324.82
Abessi and Roberts [13]	60	47.5	63.33	355.78	355.73
Abessi and Roberts [13]	60	52.5	63.25	378.53	377.54
Abessi and Roberts [13]	60	57	63.33	394.44	399.60
Abessi and Roberts [13]	60	62.5	63.13	406.88	418.13
Abessi and Roberts [13]	60	28.8	62.61	61.92	72.27
Abessi and Roberts [13]	60	31.3	62.60	255.10	260.92

Table A4
GEP results for S_r prediction

Reference	θ	*F*	*H/D*	S_r–Actual	S_r–GEP
Jiang et al. [4]	30	10.1	20	11.5	13.08
Jiang et al. [4]	30	13.5	20	16.1	15.13
Jiang et al. [4]	30	17	20	18	16.36
Jiang et al. [4]	30	20	20	17.9	17.04
Jiang et al. [4]	30	23	20	18.5	17.54
Jiang et al. [4]	30	27	20	17.7	18.02
Jiang et al. [4]	30	30	20	17.1	18.30
Jiang et al. [4]	30	32	20	17.2	18.45
Jiang et al. [4]	30	9	15	10.5	12.36
Jiang et al. [4]	30	13	15	15.3	14.40
Jiang et al. [4]	30	12.2	15	15.2	14.13
Jiang et al. [4]	30	16	15	17.9	15.13
Jiang et al. [4]	30	19	15	17	15.54
Jiang et al. [4]	30	22.4	15	17.2	15.81
Jiang et al. [4]	30	23.6	15	14.5	15.88
Jiang et al. [4]	30	25	15	16.4	15.94
Jiang et al. [4]	45	10.1	40	10	12.52
Jiang et al. [4]	45	13	40	18.2	16.80
Jiang et al. [4]	45	16.8	40	23.7	20.22
Jiang et al. [4]	45	18.7	40	23	21.44
Jiang et al. [4]	45	22.3	40	23.8	23.23
Jiang et al. [4]	45	26.2	40	25.5	24.67
Jiang et al. [4]	45	28	40	24.6	25.22
Jiang et al. [4]	45	29.9	40	25.6	25.73
Jiang et al. [4]	45	31.2	40	22.1	26.05
Jiang et al. [4]	45	34.5	40	21.3	26.77
Jiang et al. [4]	45	34.8	40	23.4	26.83
Jiang et al. [4]	45	5	25	8.47	7.78
Jiang et al. [4]	45	7.2	25	11.5	13.21
Jiang et al. [4]	45	9.1	25	14.6	15.53
Jiang et al. [4]	45	12.2	25	16.9	17.76
Jiang et al. [4]	45	14.3	25	18.2	18.73
Jiang et al. [4]	45	15.3	25	18.5	19.09
Jiang et al. [4]	45	18.1	25	18.2	19.91
Jiang et al. [4]	45	20.2	25	19.4	20.36
Jiang et al. [4]	45	22.9	25	20.9	20.82
Jiang et al. [4]	45	25.2	25	21.1	21.13
Jiang et al. [4]	45	27.2	25	20	21.36

(*Continued*)

Table A4 (*Continued*)

Reference	θ	*F*	*H/D*	S_r–Actual	S_r–GEP
Jiang et al. [4]	45	5.8	15	9.52	11.12
Jiang et al. [4]	45	7.2	15	13.3	13.37
Jiang et al. [4]	45	9.3	15	16.7	15.31
Jiang et al. [4]	45	11.1	15	18.2	16.27
Jiang et al. [4]	45	13	15	17.5	16.90
Jiang et al. [4]	45	14.1	15	17.1	17.14
Jiang et al. [4]	45	15.7	15	17.2	17.39
Jiang et al. [4]	45	17.1	15	16.4	17.52
Abessi and Roberts [13]	30	42.1	47.30	37.89	37.08
Abessi and Roberts [13]	30	43.3	47.58	35.94	37.34
Abessi and Roberts [13]	30	45.1	47.47	36.98	37.45
Abessi and Roberts [13]	30	48.1	47.16	39.92	37.55
Abessi and Roberts [13]	30	54.1	47.46	38.95	38.19
Abessi and Roberts [13]	30	32.5	37.36	33.48	31.69
Abessi and Roberts [13]	30	35	37.23	32.90	31.82
Abessi and Roberts [13]	30	37.5	37.13	33.38	31.95
Abessi and Roberts [13]	30	40	37.38	34.40	32.19
Abessi and Roberts [13]	30	42.5	37.28	32.73	32.30
Abessi and Roberts [13]	30	45	37.19	31.05	32.41
Abessi and Roberts [13]	30	50	37.31	34.00	32.73
Abessi and Roberts [13]	30	55	37.16	32.45	32.91
Abessi and Roberts [13]	30	62.5	37.20	33.13	33.26
Abessi and Roberts [13]	30	75	37.13	31.50	33.72
Abessi and Roberts [13]	30	82.5	37.16	33.83	34.00
Abessi and Roberts [13]	45	30	62.50	43.50	42.14
Abessi and Roberts [13]	45	33.1	63.65	47.66	43.12
Abessi and Roberts [13]	45	36.1	63.33	47.65	43.43

(*Continued*)

Table A4 (*Continued*)

Reference	θ	*F*	*H/D*	S_r–Actual	S_r–GEP
Abessi and Roberts [13]	45	39.1	63.06	44.57	43.72
Abessi and Roberts [13]	45	42.1	62.84	45.47	43.99
Abessi and Roberts [13]	45	48.1	63.29	48.58	44.87
Abessi and Roberts [13]	45	54.1	62.91	48.69	45.28
Abessi and Roberts [13]	45	30	62.50	40.80	42.14
Abessi and Roberts [13]	45	35	63.64	48.65	43.40
Abessi and Roberts [13]	45	37.5	63.56	43.50	43.72
Abessi and Roberts [13]	45	40	63.49	40.00	44.02
Abessi and Roberts [13]	45	42.5	63.43	39.95	44.31
Abessi and Roberts [13]	45	45	63.38	41.85	44.57
Abessi and Roberts [13]	45	50	63.29	42.50	45.07
Abessi and Roberts [13]	45	55	63.22	43.45	45.51
Abessi and Roberts [13]	45	60	63.16	47.40	45.92
Abessi and Roberts [13]	45	80	62.99	48.00	47.28
Abessi and Roberts [13]	60	60.1	79.08	54.09	52.78
Abessi and Roberts [13]	60	27.5	62.50	48.68	51.00
Abessi and Roberts [13]	60	30	62.50	47.70	50.64
Abessi and Roberts [13]	60	32.5	62.50	48.75	50.37
Abessi and Roberts [13]	60	30	62.50	52.50	50.64
Abessi and Roberts [13]	60	32.5	62.50	53.95	50.37
Abessi and Roberts [13]	60	35	63.64	46.55	47.75
Abessi and Roberts [13]	60	37.5	63.56	52.50	47.87
Abessi and Roberts [13]	60	40	63.49	50.00	47.99
Abessi and Roberts [13]	60	42.5	63.43	47.60	48.11
Abessi and Roberts [13]	60	47.5	63.33	47.50	48.33

(*Continued*)

Table A4 (*Continued*)

Reference	θ	*F*	*H*/*D*	S_r–Actual	S_r–GEP
Abessi and Roberts [13]	60	52.5	63.25	48.83	48.54
Abessi and Roberts [13]	60	57	63.33	46.74	48.59
Abessi and Roberts [13]	60	62.5	63.13	48.75	48.94
Abessi and Roberts [13]	60	67.5	63.08	47.93	49.12
Abessi and Roberts [13]	60	31.3	62.60	45.39	50.13
Abessi and Roberts [13]	60	60	63.16	47.40	48.84
Abessi and Roberts [13]	60	65	63.11	51.35	49.03
Abessi and Roberts [13]	60	70	63.06	45.50	49.21
Abessi and Roberts [13]	60	77.5	63.01	51.15	49.47